Available online at www.sciencedirect.com
SCIENCE DIRECT®
Applied Clay Science 31 (2006) 290–297
Applied CLAY Science
www.elsevier.com/locate/clay

Preparation of porous material from talc by mechanochemical treatment and subsequent leaching

Huaming Yang [a,*], Chunfang Du [a], Yuehua Hu [a], Shengming Jin [a], Wuguo Yang [a], Aidong Tang [a], E.G. Avvakumov [b]

[a] *Department of Inorganic Materials, School of Resources Processing and Bioengineering, Central South University, Changsha 410083, China*
[b] *Institute of Solid State Chemistry and Mechanochemistry, Siberian Branch of Russian Academy of Sciences, Kutateladze 18, Novosibirsk 63018, Russia*

Received 24 January 2005; received in revised form 13 October 2005; accepted 27 October 2005
Available online 2 December 2005

Abstract

Synthesis of porous silica via mechanochemical treatment of talc and subsequent acid leaching was investigated by X-ray diffraction (XRD), Fourier transformation infrared spectroscopy (FTIR), scanning electron microscopy (SEM) and N_2 adsorption techniques. Raw talc was ground for different times and then leached with 4 M hydrochloric acid (HCl) at 80 °C. Grinding for 6 h and subsequent leaching for 2 h of raw talc produced the porous silica with a specific surface area of 133 m^2/g and total pore volume of 0.22 ml/g. The increase in specific surface area (S_{BET}) of the porous silica reflected the formation of micropores of 1.2~1.8 nm and mesopores of 4.0~5.5 nm in diameter inside the porous structure. The number of micropores decreased with prolonged leaching time, which can be attributed to a condensation reaction. The characteristic of hysteresis loop indicated mainly slit-shaped pores. The apparent activation energy for the leaching process was calculated to be about 21.6 kJ/mol, indicating that the kinetic process of talc leaching was the diffusion-controlled reaction. Mechanochemical treatment may promote the amorphization of talc, being greatly favorable to the subsequent leaching.

Keywords: Talc; Porous silica; Mechanochemical treatment; Leaching; Kinetics

1. Introduction

Many special properties and broad application fields of porous materials, especially average pore size being nanometer quantity level, caused far-ranging appreciation of many scientists and enterprisers (Schüth and Schmidt, 2002). A new family of mesoporous materials is M41S which was synthesized firstly by Mobil Oil Company (Kresge et al., 1992; Chen et al., 1993; Herino, 2000). But the techniques to prepare this material need expensive organic raw materials and rigorous reaction conditions, so it is very difficult to be widely applied.

Silicate minerals are excellent raw materials for preparing porous materials because of their special structures. Much work has been done to prepare molecular sieves from zeolite type minerals which have been applied on a large scale in oil and chemistry industries (Kenneth et al., 2002; Claude, 1998; Xu and Zhu, 2003). So layer silicate minerals were used to

* Corresponding author. Tel.: +86 731 8830 549; fax: +86 731 8710 804.
E-mail address: hmyang@mail.csu.edu.cn (H. Yang).

0169-1317/$ - see front matter © 2005 Elsevier B.V. All rights reserved.
doi:10.1016/j.clay.2005.10.015

produce cheaper porous materials because of their abundant reservations. Among these layer silicate minerals, montmorillite (Veda and Krishnan, 2002; Temuujin et al., 2004) and kaolinite (Temuujin and Okada, 2002) were paid more attention.

Preparation of porous materials from silicate minerals by mechanochemical activation and subsequent leaching involves the distortion of mineral structure and the removal of metallic ions through acid leaching, leaving pores within the mineral structures. Porous materials prepared via this technique show potential applications including catalyst supports, catalyst, adsorbents and agents for organic molecule separations (Aznar et al., 1996; Suquet et al., 1991; Corma and Perez-Pariente, 1987; Gonzales et al., 1984; Okada et al., 1999). There are some examples of using acid leaching method to prepare porous silica from silicate minerals, such as metakaolinite (Okada et al., 1998), montmorillonites (Shinoda et al., 1995), antigorite (Kosuge et al., 1995), chrysotile (Suquet, 1989), phlogopite (Kaviratna and Pinnavaia, 1994), vermiculite (Temuujin et al., 2003a) and so on. The S_{BET} of leached products varies greatly from a maximum value of 670 m^2/g for vermiculite (Temuujin et al., 2003a) to about 20 m^2/g for phlogopite (Kaviratna and Pinnavaia, 1994). But no report has been focused on the kinetic behavior of the leaching process.

Clay minerals can be classified into three types: 1:1, 2:1 and 2:1:1 according to their structures and the maximum obtainable surface area. Porous materials have been prepared mainly from 1:1 and 2:1 types of clay minerals by simple acid leaching. Since the S_{BET} of the porous materials obtained from 2:1 type clay minerals are generally higher than those from the 1:1 type, the former is considered to be more desirable as raw materials for preparing porous silica. On the other hand, almost no substitution occurs in the tetrahedral layers of 2:1 clay minerals such as talc and pyrophyllite. These minerals are very resistant to acid attack (Perez Rodriguez et al., 1985; Temuujin et al., 2003b), possibly due to their unstrained structures and the presence of oxygen atoms solely between the layer surfaces. Distortion of the layer structure of talc caused by grinding may significantly promote its leaching behavior. In the present paper, the syntheses of porous silica from talc and kinetic behaviors were primarily investigated.

2. Experimental

Natural talc from Guilin, China was used as raw material. The main chemical compositions of the talc were as follows (wt.%): 62.45 SiO_2, 31.16 MgO, 0.63 Fe_2O_3, 0.08 Al_2O_3 and 0.1 TiO_2. Mechanochemical treatment was performed for different times (2, 4, 6, 8 h, respectively) in a KM-10 type planetary mill at 600 rpm at room temperature with batches of 30 g samples and 10 mm diameter stainless steel balls at a ball-to-sample weight ratio of 10:1. After batch grinding, a 2 g sample was treated with 200 ml of 4 M hydrochloric acid (HCl) at 80 °C for various times. After leaching, 100 ml of distilled water was added and the sample was allowed to cool for 30 min. The suspension was filtered and then dried at 80 °C overnight. The samples were designated as T*n*G*m*L, where *n* and *m* correspond to grinding time (h) and leaching time (h), respectively.

The crystallinity of the samples was determined by XRD (Shimadzu Labx XRD-6100). The chemical compositions were measured using X-ray fluorescence using a Rigaku RIX spectrometer. The infrared (IR) spectra were recorded with a Shimadzu FTIR 8120 spectrometer using KBr disc technique. The morphology of the samples was observed by SEM using a JEOL JSM-5310 electron microscope at an acceleration voltage of 10, 15 or 20 kV. Nitrogen gas adsorption–desorption isotherms were measured at 77 K using a Quanta Chrome Autosorb-I instrument. The specific surface area was calculated by the Brunauer–Emmet–Teller (BET) method. The total pore volume was obtained from the maximum amount of nitrogen gas adsorbed at partial pressure (p/p_0) = 0.999. Isotherm data can be derived from either desorption or adsorption isotherm to calculate the pore size distribution. A pore size distribution is defined as the distribution of pore volume with respect to pore diameter of the sample. The Kelvin equation is only suitable for pores >2 nm. Mesopore size calculations were made using the Kelvin equation. Desorption isotherm was used to determine the pore size distribution using the Barrett–Joyner–Halenda (BJH) method through the AUTOSORB software. The HK model relates relative pressure (p/p_0) to a micropore radius described by a Lennard–Jones potential. Isotherm data at very low pressure in the region of micropore filling ($p/p_0 < 0.01$) is necessary for the HK model to obtain reliable data. Micropore size distribution was derived from physisorption isotherm data according to the assumed slit-shaped pores. BJH and HK have been the commonly accepted methods to calculate the mesopore size distribution and micropore size distribution, respectively.

3. Results and discussion

3.1. Effect of milling on the talc structure

Mechanical grinding has great effect on the crystal structure of talc powder. During the grinding process, the powder surface was struck, cut and fell to pieces because of striking between the steel balls and chamber wall, which made the particle size of the powder smaller, the surface area and surface energy much higher. On the

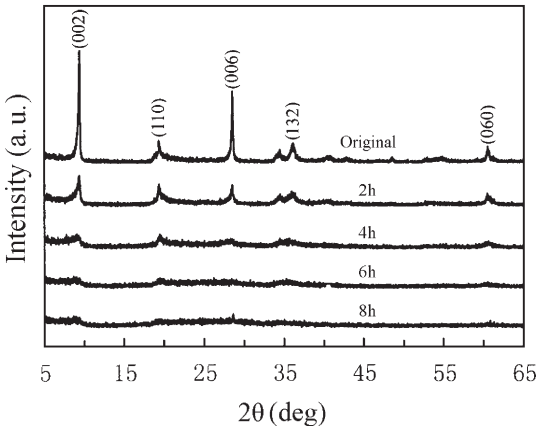

Fig. 1. XRD patterns of original talc ground for different times.

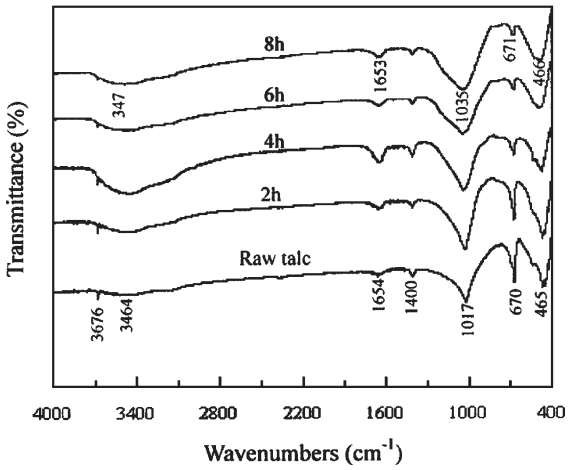

Fig. 2. FTIR spectra of raw talc ground for different times.

other hand, the chemical bonds of Si–O and Mg–O in talc were destroyed with prolonged grinding time.

The XRD patterns of the powders are shown in Fig. 1 before and after ground for different times. With the increase of grinding time, the intensities of the diffraction peaks decrease gradually and the shapes of the peaks become broad. After grinding for 6 h, some of the peaks disappear and the others become neglectable. It shows that the grinding process causes powder crystallization to decrease and surface activation increases gradually, which is favorable to subsequently leaching cations from minerals.

The crystallinity was used to quantify the progressive structural damage (Aglietti and Potto Lopez, 1992). This index includes the background and peak intensities, defining crystallinity as $C=B_0I/(I_0B)\times 100\%$, where C is the crystallinity, B_0 is the background intensity for unground material, I is the peak intensity for ground material, I_0 is the peak intensity for unground material and B is the background intensity for ground material. The results are shown in Table 1. The reflections (002), (110), (006), (132) and (060) undergo an appreciable crystallinity loss in the first 2 h; after this time, the (006), (132) and (060) reflections were too weak to be measured. After grinding for 8 h, only the reflection corresponding to the (002) plane still retains 16% of the initial intensity, indicating that prolonged grinding makes the talc amorphous.

Fig. 2 shows the FTIR spectra of the raw and ground samples. The detail assignments of each band are shown in Table 2. The grinding has a great effect on the structure of talc. The band at 3676 cm^{-1} is overlapped by a band located in 3464 cm^{-1} after grinding for 6 h. The band at 1017 cm^{-1} indicating stretching vibration of Si–O shifts to higher wave numbers. The band at 670 cm^{-1} showing stretching vibration of Si–O–Mg becomes weaker with prolonged grinding time, which is beneficial to the subsequent leaching. The band at 1400 cm^{-1} is not assigned and further research is necessary.

3.2. Leaching of the ground talc

Table 3 shows the change of chemical composition and porous properties of talc as a function of grinding time and leaching time. It is evident that the chemical composition of the ground samples changes more

Table 1
Effect of grinding time on crystallinity (%) for basal planes

Grinding time (h)	0	2	4	6	8
(002)	100	60.7	34.8	29.8	16.1
(110)	100	61.6	28.2	15.8	
(006)	100	50.4			
(132)	100	48.3			
(060)	100	35.9			

Table 2
The assignment of respective band

Vibrational frequency (cm^{-1})	Assignment
3676	Stretching vibration of Mg–OH
3429~3474	OH-stretching vibration of absorbed water
1635~1654	OH-bending vibration of absorbed water
1400	No assignment
1017~1094	In-plane stretching vibration of Si–O
670	Stretching vibration of Si–O–Mg
465~472	Bending vibration of Si–O–Si

Table 3
Variation of chemical composition and porous properties of raw talc, ground and leached samples

Sample	S_{BET} (m^2/g)	Pore volume (ml/g)	Main chemical composition (mass %)	
			SiO_2	MgO
Raw talc			60.45	31.16
Raw talc leached for 2 h	3	0.01	63.71	28.19
T2G2L			72.71	18.87
T4G2L			84.21	7.82
T6G2L	133	0.22	84.85	4.48
T8G2L	75	0.13	84.44	6.78
T6G3L	61	0.18	87.27	3.97

greatly than unground samples after leaching. The increase of SiO_2 content became more gradual above about 84%.

In the 2:1 clay minerals, the tetrahedral cations are generally the more resistant to acid attack than the octahedral cations. On this basis, Mg^{2+} ions in octahedral layer should be removed at an early stage of leaching. The XRD patterns of the raw, ground and leached samples were shown in Fig. 3. The diffraction pattern of the leached sample is similar to that of the ground sample, but with an increase in the broad feature at about 20~25°2θ arising from the presence of amorphous silica. Structural damage of the ground talc facilitates leaching of its Mg^{2+} ions, but this effect diminishes at longer grinding times. Possible reasons for this behavior include the formation of both Mg–O–Si bonds and a high agglomeration of particle structure during grinding.

SEM morphologies of the raw talc and T6G3L sample were shown in Fig. 4. SEM analysis revealed

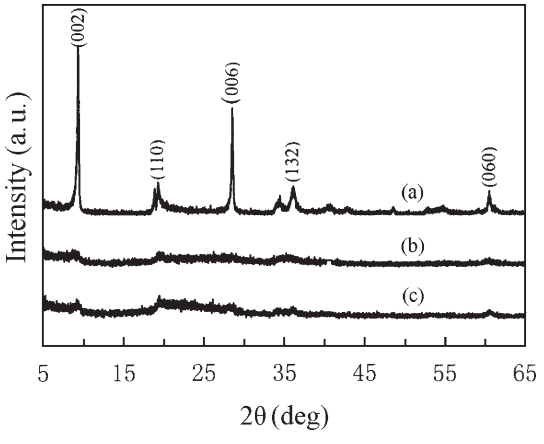

Fig. 3. XRD patterns of samples (a—raw talc, b—ground for 6 h, c—ground and after leached for 2 h).

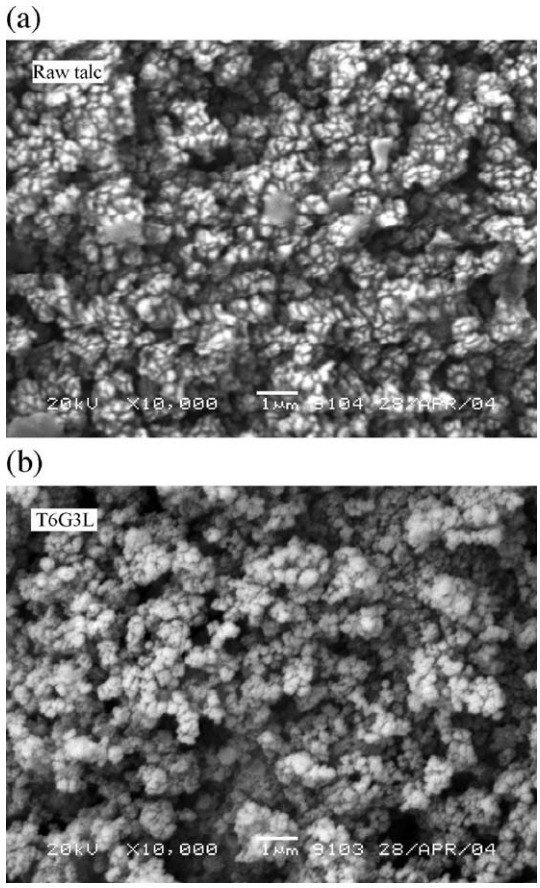

Fig. 4. SEM morphologies of raw talc and T6G3L sample (a—raw talc; b—T6G3L sample).

that the morphology of the raw talc is well retained with only a slight decrease in particle size, but the leached sample shows moderately incompact structure.

3.3. FTIR analysis

The FTIR spectra of raw talc, sample ground for 6 h and leached samples are shown in Fig. 5. A new band at 952 cm^{-1} assigned to Si–O stretching vibration of Si–OH group occurs after leaching (Kubicki et al., 1996). It is recognized that leaching transforms Si–O bands to Si–OH bands (Suquet, 1989). The presence of a band at 800~805 cm^{-1} has usually been considered as evidence for a three-dimensional amorphous silica phase (Farmer, 1974). The present intensity increase in this region at longer leaching times may suggest that removal of the octahedral cations is followed by the formation of porous silica with a three-dimensional cross-linked structure (Temuujin et al., 2004).

Leaching decreases the intensity of the absorption bands at 3676 and 670 cm^{-1} to decrease by destroying

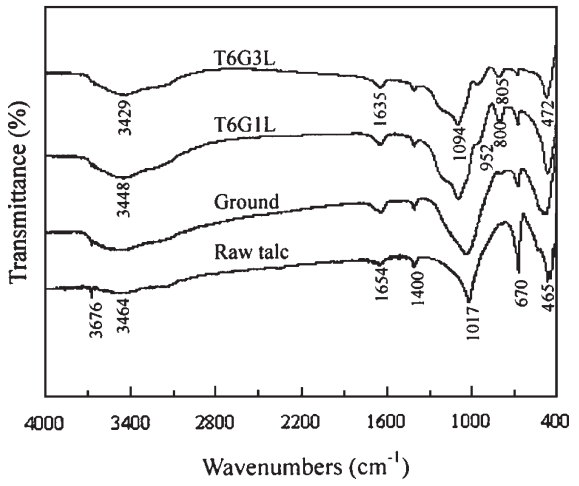

Fig. 5. FTIR spectra of raw talc, ground and leached samples (T6G3L, T6G1L).

Mg–OH bonds and partial leaching of the Mg^{2+} ions. 3429~3464 and 1635~1654 cm^{-1} are due to the OH-stretching vibrations and the OH-bending vibrations of the absorbed water, which indicate that water has no prominent effect on the IR spectra. After 3 h leaching, the Si–O bands at 1094, 805 and 472 cm^{-1} are due to the formation of an amorphous silica phase. The presence of the bands attributed to amorphous silica (1094, 805 and 472 cm^{-1}) and the Si–OH bands at 952 cm^{-1} confirm dissolution of talc treated with HCl (Madejová et al., 1998).

3.4. Porous properties

Fig. 6 shows the N_2 adsorption isotherms of the ground and leached samples. Raw talc almost has no adsorption after leaching. The presence of micropores inside the samples with grinding and leaching results in an isotherm with an initial portion resembling type I isotherms, but the remainder resembling a mixture of type II and type IV isotherms. These isotherms also show a hysteresis loop resulting from the presence of mesopores, but with no clear closure point of the desorption isotherm and the observed low pressure hysteresis. The hysteresis loop is a mixture of type H3 and type H4, indicative of narrow slit-shaped pores (Sing et al., 1985). The N_2 adsorption volume decreases with increasing grinding or leaching times, respectively, in agreement with their surface area and pore volume as shown in Table 3.

The pore size distribution (PSD) curves of the ground and leached products calculated by BJH method are shown in Fig. 7. The pore size is found to increase with increasing leaching time from less than 3 nm after leaching for 2 h to 4 nm for 3 h, the peak before 3 nm almost disappears after leaching for 3 h. The increase in pore size is greatly related to the decrease of S_{BET} with prolonged leaching time. The general trend of the PSD curves is similar to the N_2 adsorption isotherm, i.e. the maximum number of pores occurs in the samples ground for 6 h and leached for 2 h. The total amount of pores decreases with increasing grinding time. The presence of significant numbers of micropores is suggested by the extension of the curves into the micropore region, the height of which however decreased at longer grinding times. This suggests that the observed micropores not only result from leaching of the Mg^{2+} ions from the ground samples, but also include intraparticle micropores introduced by grinding.

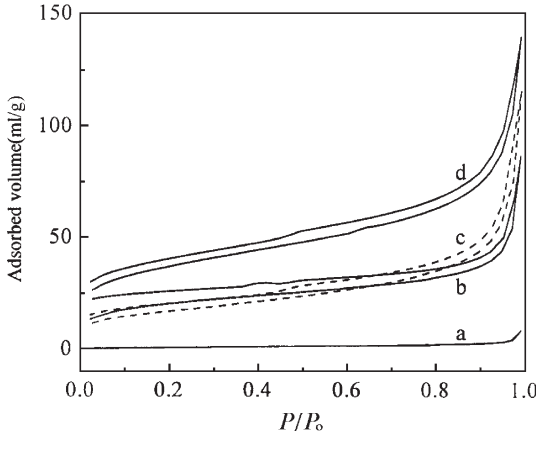

Fig. 6. N_2 adsorption–desorption isotherms (a—raw talc leached for 2 h; b—T6G3L; c—T8G2L; d—T6G2L).

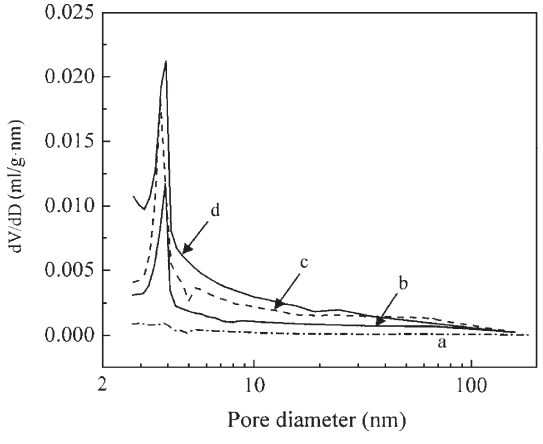

Fig. 7. PSD curves of the leached samples calculated by the BJH method (a—raw talc leached for 2 h; b—T6G3L; c—T8G2L; d—T6G2L).

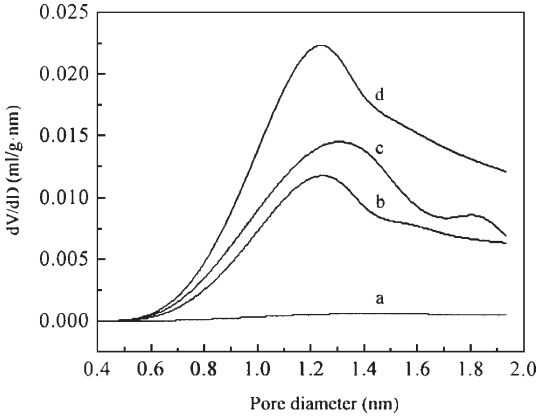

Fig. 8. PSD curves of the leached samples calculated by the HK method. (a—raw talc leached for 2 h; b—T6G3L; c—T8G2L; d—T6G2L).

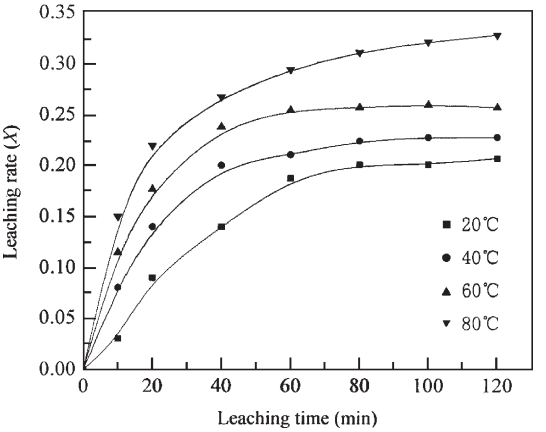

Fig. 9. Leaching rate (X) vs. leaching time at various leaching temperatures.

Fig. 8 shows the PSD curves of the leached products calculated by the HK method. The HK method is appropriate for the estimation of slit-shaped pores. Among these PSD curves, a peak was observed at a pore width of about 1.2~1.8 nm. As previous authors suggested (Okada et al., 2002; MacKenzie et al., 2004; Temuujin et al., 2001) the micropores formed by leaching of the octahedral sheets of the clay structure are rather unstable, with mesopores developing almost simultaneously by further structural rearrangement during prolonged leaching. The size of the mesopores increases further with longer leaching times. This is considered to be caused by excess leaching of the porous structure. Leaching of Mg^{2+} ions from talc begins firstly at its surface with the formation of micropores. Then micropore formation continues deeper on the surface structure with the pore size changing from micropores to mesopores and increasing in diameter from the inside to the surface with longer leaching times. The micropores partially collapse as a result of these structural alteration, which can explain the decrease of S_{BET} at prolonged leaching.

4. Kinetic investigation of leaching behavior

The leaching reaction of talc by hydrochloric acid (HCl) occurs as follows:

$$Mg_3[Si_4O_{10}](OH)_2 + 6HCl \rightarrow 3MgCl_2 + 4SiO_2{\cdot}nH_2O + (4-2n)H_2O. \quad (1)$$

The leaching rate (X) can be calculated using the following formula:

$$X = (\text{Amount of } Mg^{2+} \text{ dissolved}) / (\text{Total amount of } Mg^{2+} \text{ present in the talc}). \quad (2)$$

Fig. 9 shows the variation of the leaching rate with leaching time for different leaching temperatures as 20, 40, 60 and 80 °C for 46~74 μm particles. HCl concentration has an important influence on the leaching rate. 1 M HCl is chosen for considering the reaction rate. As a leaching agent, HCl is preferred to other acids because it allows comparatively easier recovery of the useful free acid from its waste solution. In addition, the recovery of a number of metal ions by liquid–liquid extraction from hydrochloric acid solution is considerably easier than from sulphuric acid (H_2SO_4) solutions (De et al., 1970; Tanaka, 1977).

Temperature dependence can be used to estimate the apparent activation energy. It is widely accepted that systems with an activation energy greater than 40 kJ/mol are controlled by a chemical reaction, while those with an activation energy less than 40 kJ/mol are controlled

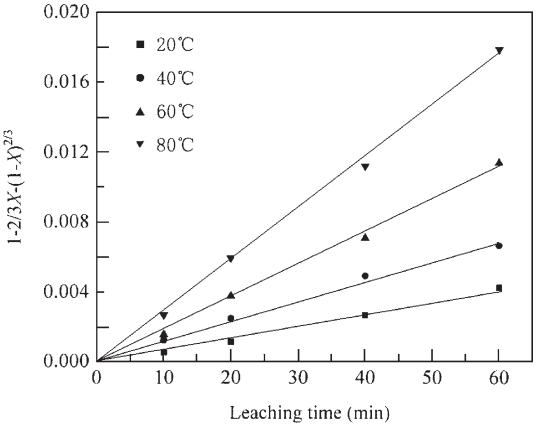

Fig. 10. Plots of $1-2/3X-(1-X)^{2/3}$ vs. time at various temperatures.

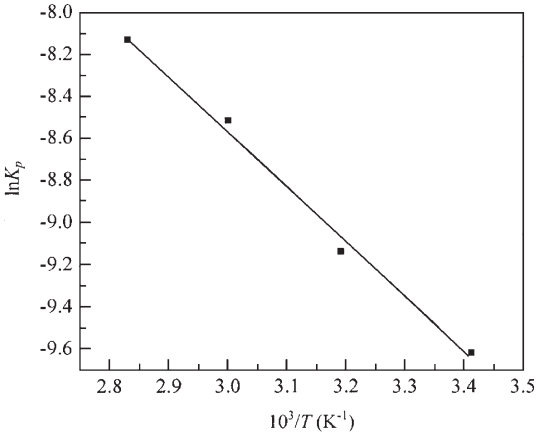

Fig. 11. Arrhenius plot for the talc leaching.

by a diffusion-controlled process, whether in the product layer or a boundary fluid film (Levenspiel, 1992). It is evident that the leaching rate of the reaction is faster in the first 60 min and it gets slower as the reaction progresses. After about 60 min, the leaching rate remains almost constant.

For the Mg^{2+} ions dissolution kinetics, two previously established shrinking core models have been used, expressed by the following equations (Dreisinger and Abed, 2002; Habashi, 1979; Sohn and Wadsworth, 1979):

$$K_c t = 1-(1-X)^{1/3} \quad (3)$$

$$K_p t = 1-2/3X-(1-X)^{2/3} \quad (4)$$

$$K_p = K_0 \exp(-E/RT) \quad (5)$$

where X is the leaching rate of Mg^{2+} ions at time t, K_c and K_p are the overall rate constants, E is the activation energy, R is the ideal gas constant and T is the leaching temperature. Eq. (3) is based on the assumption that the step controlling the leaching rate is the chemical reaction taking place on the surface of the mineral, and Eq. (4) is based on the condition that the controlling step is the diffusion process through the product layer. Examination of plots of the above kinetic equations as functions of time showed that only Eq. (4) gives perfectly straight lines in Fig. 10, the other kinetic models fail to give straight lines.

The rate constant (K_p) for the leaching reaction was calculated from the slopes of the plots in Fig. 11. The apparent activation energy calculated from the Arrhenius Eq. (5) was 21.6 kJ/mol, which is consistent with the values of activation energies reported for the diffusion-controlled reactions.

5. Conclusions

In summary, porous silica has been successfully prepared by mechanochemical treatment of talc and subsequent leaching at 80 °C. The maximum S_{BET} value achieved by this method was about 133 m^2/g with a total pore volume of 0.22 ml/g. Analysis of the pore size distribution of the leached samples indicated mainly slit-shaped micropores. The pore size changed from 1.2 nm micropores to 5.5 nm mesopores with prolonged leaching time. Structural breakdown of the ground talc facilitates the removal of Mg^{2+} ions, but this effect diminishes at longer grinding times. To obtain a porous material with a high specific surface area from mechanochemical treatment of talc, it is necessary to determine the optimal grinding conditions.

Kinetics investigation indicated that the apparent activation energy for leaching of ground talc was calculated to be about 21.6 kJ/mol, which is consistent with the values of activation energies reported for the diffusion-controlled reactions. It can be confirmed that mechanochemical treatment greatly favors the subsequent leaching of talc.

Acknowledgement

This project was supported by the National Natural Science Foundation of China (No. 50304014), the National Key Fundamental Research and Development Program of China (No. 2005CB623701), the Program for New Century 121 Excellent Talents in Hunan Province (No. 05-030119) and the Russian Foundation of Basic Researches (No. 05-03-390000).

References

Aglietti, E.F., Potto Lopez, J.M., 1992. Physicochemical and thermal properties of mechanochemically activated talc. Materials Research Bulletin 27, 1205–1216.

Aznar, A.J., Gutierrez, E., Diaz, P., Alvarez, A., Poncelet, G., 1996. Silica from sepiolite: preparation, textural properties, and use as support to catalyst. Microporous Materials 6, 105–114.

Chen, C.Y., Burkett, S.L., Li, H., 1993. Studies on mesoporous materials, synthesis mechanism of MCM-41. Microporous Materials 2, 27–34.

Claude, B., 1998. Organometallic chemistry of group VI metals in the void space of zeolites. Coordination Chemistry Reviews 178/180, 1647–1677.

Corma, A., Perez-Pariente, J., 1987. Catalytic activity of modified silicates: I. Dehydration of ethanol catalysed by acidic sepiolite. Clay Minerals 22, 423–433.

De, A.K., Khopkar, S.M., Chalmers, R.A., 1970. Solvent Extraction of Metals. Van Nostrand-Reinhold, London, pp. 23–121.

Dreisinger, D., Abed, N., 2002. A fundamental study of the reductive leaching of chalcopyrite using metallic iron: part I. Kinetic analysis. Hydrometallurgy 66, 37–57.

Farmer, V.C., 1974. Layer silicates. In: Farmer, V.C. (Ed.), The Infrared Spectra of Minerals. Mineralogical Society, London, pp. 331–363.

Gonzales, L., Ibarra, L.M., Rodriguez, A., Moya, J.S., Valle, F.J., 1984. Fibrous silica gel obtained from sepiolite by HCl attack. Clay Minerals 19, 93–98.

Habashi, F., 1979. Principles of Extractive Metallurgy, vol. 1. Gordon & Breach, New York, pp. 11–64.

Herino, R., 2000. Nanocomposite materials from porous silicon. Materials Science & Engineering. B, Solid-State Materials for Advanced Technology 69/70, 70–76.

Kaviratna, H., Pinnavaia, T.J., 1994. Acid hydrolysis of octahedral Mg^{2+} sites in 2:1 layered silicates: an assessment of edge attack and gallery access mechanism. Clays and Clay Minerals 42, 717–723.

Kenneth, J.B., Godefroy, G., Deng, Z., 2002. Preparation of partially oriented zeolite MCM-22 membranes via pulsed laser deposition. Microporous and Mesoporous Materials 52, 41–150.

Kosuge, K., Shimada, K., Tsunashina, A., 1995. Micropore formation by acid treatment of antigorite. Chemistry of Materials 7, 2241–2246.

Kresge, C.T., Leonowicz, M.E., Roth, W.J., 1992. Ordered mesoporous molecular sieves synthesized by a liquid–crystal template mechanism. Nature 359, 710–716.

Kubicki, J.D., Blake, G.A., Apitz, S.E., 1996. Ab initio calculations on aluminosilicate Q3 species: implication for atomic structures of mineral surfaces and dissolution mechanism of feldspars. American Mineralogist 81, 789–799.

Levenspiel, Q., 1992. Chemical Reaction Engineering, 2nd ed. Wiley, New York, NK, pp. 23–49.

MacKenzie, K.J.D., Okada, K., Temuujin, J., 2004. Nanoporous inorganic materials from mineral templates. Current Applied Physics 4, 167–170.

Madejová, J., Bujdák, J., Janek, M., Komadel, P., 1998. Comparative FT-IR study of structural modifications during acid treatment of dioctahedral smectites and hectorite. Spectrochimica Acta Part A 54, 1397–1406.

Okada, K., Shimai, A., Takei, T., Hayashi, S., Yasumori, A., MacKenzie, K.J.D., 1998. Preparation of microporous silica from metakaolinite by selective leaching method. Microporous and Mesoporous Materials 21, 289–296.

Okada, K., Shimai, A., Hayashi, S., Yasumori, A., 1999. Adsorption properties of microporous silica prepared from metakaolinte by selective leaching method. Clay Science 11, 73–82.

Okada, K., Nakazawa, N., Kameshima, Y., Yasumor, A., 2002. Preparation and porous properties of materials prepared by selective leaching of phlogopite. Clays and Clay Minerals 50, 624–632.

Perez Rodriguez, J.L., Maqueda, C., Justo, A., 1985. Pyrophyllite determination in mineral mixture. Clays and Clay Minerals 33, 563–566.

Schüth, F., Schmidt, W., 2002. Microporous and mesoporous materials. Advanced Materials 14, 629–638.

Shinoda, T., Onaka, M., Izumi, Y., 1995. Proposed models of mesopore structures in sulfuric acid-treated montmorillonites and K10. Chemistry Letters 24, 495–496.

Sing, K.S.W., Everett, D.H., Haul, R.A.W., et al., 1985. Reporting physisorption data for gas/solid systems with special reference to the determination of surface area and porosity. International Union of Pure and Applied Chemistry 57, 603–619.

Sohn, H., Wadsworth, M.E., 1979. Rate Process of Extractive Metallurgy. Plenum, New York, pp. 141–143.

Suquet, H., 1989. Effect of dry grinding and leaching on the crystal structure of chrysotile. Clays and Clay Minerals 37, 439–445.

Suquet, H., Chevalier, S., Marcilly, C., Barthomeuf, D., 1991. Preparation of porous materials by chemical activation of the Llano vermiculite. Clay Minerals 26, 49–60.

Tanaka, M., 1977. Chemistry of Solvent Extraction. Kyoritsu, Tokyo, pp. 2–38.

Temuujin, J., Okada, K., 2002. Zeolite formation by hydrothermal treatment of waste solution from selective leached kaolinite. Materials Letters 52, 91–95.

Temuujin, J., Okada, K., MacKenzie, K.J.D., Jadambaa, T., 2001. Characterization of porous silica prepared from mechanically amorphized kaolinite by selective leaching. Powder Technology 121, 259–262.

Temuujin, J., Okada, K., MacKenzie, K.J.D., 2003a. Preparation of porous silica from vermiculite by selective leaching. Applied Clay Science 22, 187–195.

Temuujin, J., Okada, K., Jadambaa, T., MacKenzie, K.J.D., Amarsanaa, J., 2003b. Effect of grinding on the leaching behaviour of pyrophyllite. Journal of the European Ceramics Society 23, 1277–1282.

Temuujin, J., Jadambaa, T., Burmaa, G., 2004. Characterisation of acid activated montmorillonite clay from Tuulant (Mongolia). Ceramics International 30, 251–255.

Veda, R., Krishnan, M.S., 2002. Immobilization and characterization of copper chlorophthalocyanine on alumina-pillared montmorillonite. Journal of Molecular Catalysis A 181, 81–89.

Xu, Y., Zhu, J.H., 2003. Removing nitrosamines from mainstream smoke of cigarettes by zeolites. Microporous and Mesoporous Materials 60, 125–138.